CEBAF Program Advisory Committee Nine Proposal Cover Sheet

This proposal must be received by close of business on Thursday, December 1, 1994 at:

CEBAF

User Liaison Office, Mail Stop 12 B

12000 Jefferson Avenue

Newport News, VA 23606

Proposal Title

SEARCH FOR JPC = 1-+ EXOTIC MESONS IN THE ELECTROPRODUCTION REACTIONS USING CLAS DETECTOR AT CEBAF.

Contact Person

Name: Stepan Stepanyan

Institution: Yerevan Physics Institute

Address: Alikhanian Brothers St.2, Yerevan 375036, Armenia.

Address: 12000 Jefferson Av.

City, State ZIP/Country: Newport News, VA 23606, USA

Phone: (804) 249 - 7196 **FAX:** (804) 249 - 6273

E-Mail → Internet: Stepanyan@CEBAF.Gov

Experimental Hall: B **Days Requested for Approval:** 30

Hall B proposals only, list any experiments and days for concurrent running:

NA

CEBAF Use Only

Receipt Date: 12/15/94 PR 94-118

By: SP

SEARCH FOR $J^{PC} = 1^{-+}$ EXOTIC MESONS IN THE ELECTROPRODUCTION REACTIONS USING CLAS DETECTOR AT CEBAF *

W.BROOKS, V.BURKERT, D.CORDS, A.FREYBERGER,
B.MECKING, M.MESTAYER, B.NICZYPORUK, E.SMITH
CEBAF
Newport News, VA 23606

I.AZNAURYAN, G.ASRYAN, R.DEMIRCHYAN, H.EGIYAN,
K.EGIYAN, M.SARGSYAN, S.STEPANYAN, Yu.SHARABYAN
Yerevan Physics Institute
Yerevan, Armenia

A.COLEMAN, H.FUNSTEN, K.GRIFFIOEN, T.Y.TUNG
The College of William and Mary
Williamsburg, VA 23187

G.ADAMS
Rensselaer Polytechnic Institute
Troy, NY 12180

CLAS COLLABORATION

Spokespersons: I.Aznauryan, Herbert Funsten, Stepan Stepanyan

ABSTRACT

This experiment will search for $J^{PC} = 1^{-+}, J^{PG} = 1^{--}$ exotic hybrids in electroproduction in the mass range up to ≈ 2 GeV by detection of the $\eta\pi$, and $\eta'\pi$, pseudoscalar meson decay products. The signature for the exotic will be obtained from the measurement of the angular distributions of the reconstructed pseudoscalar mesons. There have been indications of these hybrids in hadronic production. Using estimates of the electroproduction cross section and the exotic hybrid branching fraction into $\eta\pi$ we expect ~ 10000 reconstructed hybrids in a 30 day running period with a $6\ GeV\ e^-$ beam.

*Proposal for PAC9

1. Introduction

The gluon, the QCD gauge boson, carries color charge. It can have a component characterizing it as a force and a component characterizing it as a constituent particle[1]. It can thus act as a particle and experience a binding force to quarks arising from additional gluons interconnecting to the quarks. One thus expects a class of hadrons, hybrid mesons, comprised of a valence gluon bound to two quarks, $gq\overline{q}$. (In addition, there are expectations for the existence of a glueball meson consisting of a gluon loop, gg and for existence of hybrid baryons $gqqq$). QCD models have made a variety of predictions of the masses, widths, and decays of hybrid $gq\overline{q}$[1,2,3,4,5,6]. Although evidence for gluons has been found in jet measurements and in deep inelastic scattering, an unambiguous signal of constituent glue has not been observed. The discovery of hybrids would be a strong confirmation of QCD and important for understanding the non-perturbative structure of hadrons.

A subset of the J^{PC} / J^{PG} hybrid exotics, has a simple detection signature. A bound system consisting of only a fermion - antifermion pair, i.e., a $q\overline{q}$ system, lacks some members of its J $\geq$ 1 positive naturality (i.e., J^P =1^-, 2^+, 3^-, etc) states. For a neutral meson, states with $P \neq C$ will be lacking. These states have "exotic" quantum numbers and must have a constituent boson in addition to a $q\overline{q}$ pair, i.e., the state is a hybrid. For a charged meson of isospin I, states with $G = (-1)^I P$ will be exotic.

The detection of a state with the exotic quantum quantum numbers $J^{PC} = 1^{-+}$ or $J^{PG} = 1^{--}$, denoted by $\hat{X}$, then unambiguously indicates a hybrid. Although nonexotic hybrids (i.e., hybrids with conventional quantum numbers) exist, disentangling them from $q\overline{q}$ states with the same quantum numbers is difficult. Furthermore, nonexotic hybrid - $q\overline{q}$ mixing may be appreciable.

In experimentally detecting exotic hybrids, the additive quantum number C/G is determined by final state particle identification. A determination of J and P from the meson's angular decay distribution pattern, W, can then yield the existence of a $J^{PC/G}$ hybrid exotic.

Most of the searches for exotics have used hadronic production, i.e., $\pi^- p$ and $p\overline{p}$ reactions characteristically yielding high statistics data. J/ψ decays have been studied, but with considerably lower statistics. e^+e^- reactions have been used to search for exotic production via a 2γ process, although exotic production cross sections are not expected to differ with that for hadronic production [7].

Since a charged pion and a photon in a relative P wave (l = 1) can couple to the $J^{PG} = 1^{--}$ exotic quantum numbers, electromagnetic production of these exotics by t-channel pion exchange may be competitive with hadronic production. Several experiments have investigated coherent nuclear production from incident charged π in the intense coulombic field of a high Z nucleus (Primakoff - like production). Experimental results for Primakoff production have been inconclusive.

2. Theoretical Predictions and Existing Data

Theory

Predictions have been made for hybrids in several different QCD models and have been presented in hadron spectroscopy workshop proceedings [8] and reviews[9]. All models in general predict $J^{PC} = 1^{-+}$ and $J^{PG} = 1^{--}$ hybrids with masses at or below $2.0 GeV$ [4,5,6,10,11]. Widths in the range $\Gamma \sim 50 \rightarrow 200 MeV$ are favored. The predicted decay modes are uncertain. In some models, gluonic excitation does not transfer its spin to the final state mesons' relative orbital angular momentum and hybrid decay to two mesons with quark S-waves does not occur. However, other models [10,12,13,14] predict such decay. It occurs through such effects as spurious bag CM motion[10], or through the sequential decay of the exotic hybrid into a nonexotic hybrid and then into a conventional meson via mixing[14]. The nonexotic hybrid is mixed with a conventional meson which appears in the final state. In this description the $\pi\eta(\eta')$ have small constituent gluonic components. In general $Br_{\eta\pi} \sim 0.1$ and $Br_{\eta\pi}/Br_{\eta'\pi} \sim 1/3$ is predicted.

Existing Data

Several experiments have examined the decay angular distribution in the $\pi\eta(\eta')$ final states in hadronic production in order to detect $J^{PC} = 1^{-+}$ and $J^{PG} = 1^{--}$ exotic hybrid states. Although their results have not been conclusive, there is general indication of the existence of these states. (The subscript on a decay partial wave value indicates the naturality of a t-channel exchange in the limit $s \rightarrow \infty$, $0, -$ indicates negative naturality, $+$ is positive).

a) *GAMS Experiment (CERN)* [15]
The reaction

$$\pi^- p \rightarrow \hat{X}^0 n; \; \hat{X}^0 \rightarrow \pi^\circ \eta$$

was studied at the CERN SPS with a 100 GeV/c negative pion beam using the GAMS-4000 lead-glass hodoscopic calorimeter. The mass range $1.2 \leq m_{\hat{X}^0} \leq 1.6$ GeV was examined. Partial wave analysis (PWA) of this data shows a clear $a_2(1320)$ D_0 wave in the $\eta\pi^\circ$ system and a resonant structure in the P_0-wave at a mass 1.4 GeV (Fig.1a). Forward-backward asymmetry of the decay angular distribution in the Gottfried-Jackson frame of the $\eta\pi^\circ$ system was observed (Fig.1b). This is indicative of interfering D and P waves. The resonance was ascribed to a $\hat{\rho}(1405)$ exotic. Questions, however, have arisen about the analysis (see Sec.4).

b) *KEK Experiment* [16]
Forward-backward decay asymmetry in $\hat{X}^- \rightarrow \pi^-\eta$ has also been seen in the

reaction

$$\pi^- p \rightarrow \hat{X}^- n;\ \hat{X}^- \rightarrow \pi^- \eta$$

at 6.3 GeV/c beam momentum(Fig.2a). PWA, as in GAMS, showed a clear D-wave of the $a_2(1320)$ and a resonant structure in the P-wave (Fig.2b). $m_{\hat{X}^0} \approx 1.32\ GeV$; obtained by a Breit-Wigner fit to the P_+-wave. (This is 0.1 GeV less than that obtained by GAMS.

c) *Fermilab Experiment E272* [17,18,19]

A Primakoff production experiment has been carried out at Fermilab using a 202.5 GeV energy π^+ beam interacting with heavy nuclear targets (Pb, Cu). The measured reactions were:

$$\pi^+ A \rightarrow \hat{X}^+ A\ ;\ \hat{X}^+ \rightarrow \rho\pi^+;\ \eta\pi^+;\ D(1285)\pi^+$$

The data showed that neither $\rho^0\pi^+$ nor $\eta\pi^+$ are likely to be major decay modes of a hybrid with a mass below 1.5 GeV and width larger than 20 MeV. Upper limits of $Br(\hat{X}^+ \rightarrow \rho\pi^+)$ of a few percent and $\Gamma(\hat{X}^+ \rightarrow \gamma\pi^+) \cdot Br(\hat{X}^+ \rightarrow \eta\pi^+) \sim 15 - 25keV$ (Fig.3a,b) were obtained in the experiment[20]. The $D(1285)$ π^+ data indicated a relatively narrow structure at 1.6 GeV (Fig.3c). However J^P of this mode has not been determined.

d) *VES Experiment (IHEP)* [21]

Possible $\hat{X}^-$ decays to $\eta\pi^-$ and $\eta'\pi^-$ systems were studied in a high-statistics experiment at the IHEP VES setup using a π^- beam at momentum $p_{\pi^-} = 37GeV$ on a beryllium target. The reactions studied were:

$$\pi^- N \rightarrow \hat{X}^- N;\ \hat{X}^- \rightarrow \pi^-\eta(\eta')$$

Partial-wave analysis were done for both reactions.

In the $\eta\pi^-$ system the $a_2^-(1320)$ D_+ wave was dominant. A P_+ wave with exotic quantum numbers appeared as a small, broad bump at mass $M_{\eta\pi^-} \approx 1.4\ GeV$ (see Fig.4a).

In the $\eta'\pi^-$ system the intensity of the D_+ wave was small (branching ratio $BR(a_2 \rightarrow \eta'\pi) \leq 0.01$). The largest wave in this system was P_+ (Fig.4b).

The intensity of P_+ waves in the both systems is shown in Fig.5. The authors[21] conclude that the $q\bar{q}g$ system could be the main component of P_+ wave. The relative strengths are consistent with a valence gluon hybrid, $q\bar{q}g$, with $J^{PG} = 1^{-+}$ predicted by Close and Lipkin[12].

e) *Photoproduction Experiments* [22,23]

Photoproduction data of hybrids is sparse. There are two reported experiments on photoproduction of hybrids that are not necessarily J^{PC} exotics. Final state meson systems other than $\pi\eta$ (η') were observed. There are no reported electroproduction experiments.

The first experiment was diffractive photoproduction of $b_1\pi$ system[22]. There were two resonant structures for $m_{b_1\pi} \geq 1.5\ GeV$, Fig.6. The first structure was interpreted as the $\omega_3(1670)$. The second had a centroid mass of 1.8 GeV and a width $\leq 0.3\ GeV$. It was interpreted as a gluonic hybrid.

The second experiment was photoproduction of an isovector $\rho\pi$ meson system [23]. A resonant structure was observed at an invariant mass of $(\rho\pi)$ 1.775 GeV(Fig.7a). The structure can not be interpreted as a $\pi_2(1670)$ due to significant mass shift ($\sim 100\ MeV$) and dominant $\rho\pi$ coupling (Fig.7b). The angular distribution of the decay in the Gottfried-Jackson frame was consistent with $J^P = 1^-; 2^-; 3^+$.

3. Proposed Experiment

The experiment we propose is electroproduction of $\hat{X}$, with isospin 1, $J^{PC} = 1^{-+}$ and $J^{PG} = 1^{--}$exotic hybrid from a hydrogen target. In electromagnetic production hybrids may be produced via vertices that do not exist in hadroproduction. Electroproduction allows measurements of couplings to polarization states not accessible with either a pion or real photon beam. Furthermore transition form factors can be measured. Electroproduction is the complement to the above Primakoff production method. The photon is now incident on the pionic field of a nucleon. The lack of a large nuclear coulombic field is compensated by a high incident flux of virtual photons.

We propose to use the CLAS to search for exotic hybrids in the $\pi^+\eta(\eta')$ and $\pi^0\eta(\eta')$ decay channels at $E_e = 6\ GeV$ beam energy. Reactions to be studied are:

$$ep \rightarrow e'\hat{X}^+n;\ \hat{X}^+ \rightarrow \pi^+\eta(\eta') \tag{1}$$

$$ep \rightarrow e'\hat{X}^0p;\ \hat{X}^0 \rightarrow \pi^0\eta(\eta') \tag{2}$$

where $\hat{X}^{\binom{+}{0}}$ are the charged/neutral $J^{PC} = 1^{-+}$/ $J^{PG} = 1^{--}$exotic hybrid mesons. One photon exchange diagram of reactions (1) and (2) are presented in Fig.8. Measurements will be done in the hadronic mass range $W \geq 2.6GeV$ and $Q^2 \geq 0.7(GeV/c)^2$. These final state mesons π, η, η', will insure the desired G / C parity of the decaying meson.

The ability of the Hall B CLAS spectrometer to detect multiparticle final states will allow determination of the J and P from the angular distribution, $W(\theta, \phi, \Phi)$ of the pseudoscalar decay. Here θ is the decay polar angle, ϕ is the angle between the decay and hadron CMS planes and Φ is the angle between electron and hadron CMS planes (see Fig.9).

$W(\theta, \phi, \Phi)$ uniquely determines J and P since the relative orbital angular momentum of the two pseudoscalar mesons, characterizing $W(\theta, \phi, \Phi)$, equals J. The equality would not exist if the mesons had non-zero spin. $W(\theta, \phi, \Phi)$ also determines the polarization of the hybrid meson, i.e., the measurement is polarization "self analyzing". A second scattering measurement is not needed.

The polarization will indicate the electroproduction mechanism. For example if electroproduction is predominately by t-channel exchange of a spinless particle, e.g., a pion, the polarization determined by evaluating $W(\theta, \phi, \Phi)$ in the Gottfried -Jackson frame[24] will be that of the incident virtual photon as seen in this frame.

The C/G, J, P measurement will then identify a $J^{PC} = 1^{-+}$ or $J^{PG} = 1^{--}$ exotic.

Under some conditions, additional information can be obtained from the dependence of $W(\theta, \phi, \Phi)$ on the $m_{\pi\eta(\eta')}$ invariant mass. This occurs when a electroproduced meson, M, has a mass lying nearby $m_{\hat{X}}$. If M decays into the same final states into which the $\hat{X}$ decays, the electroproduction amplitudes for $\hat{X}$ relative to those of M can be obtained from the interference terms in $W(\theta, \phi, \Phi)$(see Sec.8.2). An example in the mass region $1.2 - 1.4\ GeV$ is the $a_2(1320)$ meson which has a $\approx 15\%$ branching ratio into $\eta\pi$. Additional measurements of $W(\theta, \phi, \Phi)$ at the $a_2(1320)$ mass centroid yield amplitudes characteristic of direct $a_2(1320)$ electroproduction . These can then be used with those obtained in the interference mass region to obtain absolute $\hat{X}$ production amplitudes.

4. Production Mechanism and Decay Analysis

The predominant electromagnetic production mechanisms of $J^{PG} = 1^{--}$states can be estimated for forward scattering by using values of allowed hadronic couplings and VMD.

Electromagnetic production of positive $J^{PG} = 1^{--}$ mesons will proceed via the diagrams in Fig.10a. In our experiment we expect forward production of positive $J^{PG} = 1^{--}$ (also $a_2(1320)$) to proceed predominantly via π^+ exchange because of the large πNN coupling.

Electromagnetic production of neutral $J^{PG} = 1^{--}$ mesons can go only through the C-odd exchanges of ω and ρ (see diagrams Fig.10b). The left diagram in Fig.10b is dominant at small momenta transfers because:

(a) the coupling constant $g_{\omega pp}$ is larger than $g_{\rho pp}$: $g_{\rho pp} \simeq 4 \cdot g_{\omega pp}$ [25]

(a) the coupling constant $g_{\rho\gamma}$ is larger than $g_{\omega\gamma}$: $g_{\rho\gamma} \simeq 3 \cdot g_{\omega\gamma}$.

Since spin nonflip $g^V_{\omega pp}$ is much larger then spin flip $g^T_{\omega pp}$, in the forward direction the $\hat{X}$ polarization equals that of the virtual photon. Production of neutral $J^{PC} = 1^{-+}$system is dominated at small momentum transfer by spin-nonflip natural parity exchange (NPE).

In the analysis of the GAMS experiment $\pi^- p \to \pi^0\eta n$[15], the exotic state $J^{PC} = 1^{-+}$ appears in the amplitude P_0, i.e. its production mechanism corresponds to unnatural parity exchange (UPE). At the same time, at the energies used in the experiment ($100GeV$) the main contribution is expected to be ρ-exchange i.e. natural parity exchange (NPE). This was confirmed in the KEK[16] and VES[21] experiments, where in the reaction $\pi^- p \to \pi^-\eta(\eta')$ an exotic appears in the P_+ amplitude (NPE).

For this reason the results of the partial wave analysis of data from [15] are doubtful.

Decay analysis is simplified by the spins of the final states. These zero spins will uniquely determine the J and P of the exotic by measurement of the decay angular distribution, $W(\theta, \phi, \Phi)$.

Determination of $W(\theta, \phi, \Phi)$ will be done in an appropriate Lorentz frame. As noted previously, if pion t-channel exchange is predominant, the Gottfried - Jackson frame greatly simplifies analysis. Full analysis of cross section dependence from density matrices for electroproduction of spin one particles are given in Ref.[26,27,28]. Calculations of the expected sensitivities to the production amplitudes in electroproduction are in progress. Estimates of the sensitivities in the photoproduction can be found in Appendix A.

5. Kinematics

The kinematics of the proposed experiment is based on the expected exotic's mass range ($m_{\hat{X}} \approx 1.2\ GeV \rightarrow 2.0\ GeV$).

A 6 GeV beam energy is required to cover the masses of interest.

In Fig.11a obtainable ranges of W and Q^2 are shown. The CLAS magnetic field was set at 1/2 nominal value in order to detect the range of the scattered electrons, bending inwards the toward the beam axis. Lowering the magnetic field has little effect on the resolution of reconstructed mass and angles which is dominated by the electromagnetic calorimeter resolution for the final states photons.

The $\hat{X}$ mass range necessitates $W \geq 2.6$ GeV; the maximum value of W is 3.1 GeV. The $\hat{X}$ mass range is shown in Fig 11b. Corresponding ranges of the scattered electron energy and polar angle are shown in Fig. 11c. The $m_{\hat{X}}$ dependence of t_{min} is shown in Fig. 11d for the above range of W (t_{min} is the minimum value of 4 - momentum transfer at the hadron scattering vertex).

Low values of t_{min} result in high cross section values, particularly if t - channel pion exchange predominates.

The kinematic variables ν, Q^2 and W will be determined by detection of the scattered electron. The four-momenta of the $\hat{X}$ will be reconstructed from the detected π^+ and reconstructed η or η' decay mesons in reaction (1) and from the detected proton in reaction (2).

Vertex definition will not be problem since in all proposed reactions there are at least two charged particles in the final states.

6. Acceptance Simulations

As noted above, the hybrid exotics will be studied via decay modes: $\pi^+\eta$, $\pi^+\eta'$, $\pi^0\eta$ and $\pi^0\eta'$. Reconstruction of π^0 and η mesons will be done by detection of their two photon decay in the CLAS electromagnetic shower calorimeter. For the η mesons the two photon decay branch is $Br(\eta \rightarrow \gamma\gamma) = 0.39$. η' reconstruction will be by the $\rho\gamma$ decay mode ($Br(\eta' \rightarrow \rho\gamma) = 0.3$). The final detected particles in the reactions (1) and (2) are:

(1) $\hat{X}^+ \Rightarrow \pi^+\eta$: $e'\,\pi^+\,\gamma\,\gamma$
$\hat{X}^+ \Rightarrow \pi^+\eta'$: $e'\,\pi^+\,\pi^+\,\pi^-\,\gamma$
(2) $\hat{X}^0 \Rightarrow \pi^0\eta$: $e'\,p\,\gamma\,\gamma\,\gamma\,\gamma$
$\hat{X}^0 \Rightarrow \pi^0\eta'$: $e'\,p\,\pi^+\,\pi^-\,\gamma\,\gamma\,\gamma$

Event simulation and reconstruction in the CLAS was performed using the SDA program [29]. The CLAS electromagnetic calorimeter γ response was simulated by use of the GEANT[30] and EC[31] codes. The resulting γ response was parameterized and incorporated into the SDA simulations.

An event generator was written to simulate t-channel photo- and electroproduction from a proton target. The t behavior of the cross section and decay angular correlation, $W(\theta, \phi, \Phi)$, was determined .

Events were generated as functions of W, (hadron vertex cm energy), Q^2, (γ_V invariant mass squared), Φ (electron - hadron plane angle), $m_{\hat{X}}$, t, and Ω_{GJ}, (spherical angle of decay mesons in the Gottfried-Jackson frame).

Calculations of acceptances and resolutions for each of the four final states were made at $W = 3.0\ GeV$ and $Q^2 = 1.0\ (GeV/c)^2$, the average minimum Q^2 for $W = 2.6 \rightarrow 3.1\ GeV$, at 6 GeV beam energy and for 1/2 magnetic field.

A typical CLAS event pattern for a $ep \Rightarrow p\pi^+\gamma\gamma$ reaction is shown in Fig.12

Acceptances for the reactions (1) are shown in Fig.13 and 14. Similar results were obtained for the reaction (2). The acceptances vary smoothly with $m_{\hat{X}}$, t, and Ω_{GJ}. There are no gaps in Ω_{GJ}, important in partial wave analysis. The acceptance for the $\pi^+\eta$ final state, $A_{\pi^+\eta} \approx 11\%$. Acceptances for the other final states were: $A_{\pi^+\eta'} \approx 4\%$; $A_{\pi^0\eta} \approx 4.5\%$; and $A_{\pi^0\eta'} \approx 1\%$. In this calculations, 3σ cuts were used on all three reconstructed masses ($\sigma_{\pi^0} = 17\ MeV$, $\sigma_\eta = 35\ MeV$ and $\sigma_{\eta'} = 20\ MeV$).

Two photon invariant mass distributions, $m_{\gamma\gamma}$, for π^0 (dashed histogram) and η (solid histogram) are shown in Fig.15a. Reconstructed mass of η' is shown in Fig.15b.

In reactions (1) the outgoing neutron is not detected. To suppress background, discussed later, a cut was made on the neutron missing mass. This eliminated semi-inclusive $\pi\eta(\eta')$ final states accompanied by high multiplicity.

The simulated mass, t, θ_{GJ} and ϕ resolutions for $\hat{X}^+$ are shown in Fig.16 and 17. For the neutral $\hat{X}^0$ reactions in (2), we use the proton information for mass and t

reconstruction. It significantly improves the resolution (see Fig.18). Distributions for θ_{GJ} and ϕ remain the same.

7. Cross Section and Counting Rate

There is no reported data on electromagnetic production of the $J^{PC} = 1^{-+}$ hybrid. However $a_2(1320)$ $(J^{PC} = 2^{++})$ photoproduction data and measured upper limits to Primakoff nuclear $J^{PC} = 1^{-+}$hybrid production exist [20]. From these the estimated photoproduction cross section $\sigma^{\gamma}_{\hat{X}} = 0.9\ [m]b$ (see Appendix B).

The estimated $\hat{X}$ photoproduction cross section can be extended to electroproduction (see Appendix B):

$$\frac{d^2\sigma_{ep\to \hat{X}^+ n}}{dQ^2 dW} = \Gamma_e \cdot F_\rho \cdot \sigma^{\gamma}_{\hat{X}} \tag{3}$$

where Γ_e is the Mott cross section and F_ρ is a factor based upon $\gamma \to \rho$ VMD conversion.

For $W = 3.0\ GeV$ and $Q^2 = 1.0\ (GeV/c)^2$, $\Gamma_e \cdot F_\rho = 3 \cdot 10^{-4}$. This yields a cross section is $\approx 2.7 \cdot 10^{-4}\ \mu b \cdot (GeV/c)^{-3}$.

For comparison, the inclusive (ee') cross section at $Q^2 = 1.(GeV/c)^2$ and $W = 3.\ GeV$ is $3 \cdot 10^{-2} \mu b \cdot (GeV/c)^{-3}$.

Table 1 shows the estimated count rates for $\Delta W = 0.6\ GeV$ and $\Delta Q^2 = 0.5\ (GeV/c)^2$ and 30 days running period with $E_e = 6\ GeV$ electron beam on hydrogen target at total luminosity $L = 10^{34}\ cm^{-2} sec^{-1}$.

Table 1: Count Rates for 30 Days Running Period at $L = 10^{34}$

Process	Decay Modes and Br. Ratios				Acc.	Counts
$ep \to e'\hat{X}^+$	$\hat{X} \to \eta\pi^+$	0.1	$\eta \to \gamma\gamma$	0.39	0.11	10000
$ep \to e'\hat{X}^+$	$\hat{X} \to \eta'\pi^+$	$0.3 : 1.4^{\dagger}$	$\eta' \to \pi^+\pi^-\gamma$	0.3	0.04	6000
$ep \to e'a_2^+ n$	$a_2^+ \to \eta\pi^+$	0.15 :	$\eta \to \gamma\gamma$	0.39	0.11	35000

† Using $Br(\hat{X}^+ \to \pi^+\eta') = 3 \cdot Br(\hat{X}^+ \to \pi^+\eta)$ and phase space factor for η' of 1.4.

8. Background

Coherent and incoherent background for $\hat{X}$ identification will arise from multiparticle final state events. For example, in the electromagnetic shower calorimeter one

photon from each π^0 in a $\pi^+\pi^0\pi^0$ final state can be confused with a $\pi^+\eta \rightarrow \pi^+\gamma\gamma$ final state. This incoherent background, as shown below, can be minimized by narrow kinematic cuts.

8.1. Incoherent Background

Incoherent background was estimated for the final states in reaction (1) using CELEG code[32] as an event generator. The program includes baryon resonances up to $\sim 2.GeV$ in mass. In the deep inelastic region CELEG uses the Lund Monte-Carlo program LEPTO[33]. The relatively large value of W (W$\geq$ 2.6 GeV) needed for this experiment results in background arising predominately from the deep inelastic scattering region rather than the resonance region.

A total of $2\cdot10^5$ ep interactions were generated in the range of $W = 2.6 \rightarrow 3.1GeV$ and $Q^2 \geq 0.7(GeV/c)^2$. The ratio of differential cross sections for reaction $ep \rightarrow e'\hat{X}^+$ and ee' is $\approx 10^{-2}$ (see Sec.7). After simulation of the CLAS detector efficiency for these events the final states were reconstructed. The two photon invariant mass spectrum from final states that have $e'\pi^+\gamma\gamma$ tracks, (total 461 events) is shown in Fig.19a. Clearly seen two $m_{\gamma\gamma}$ mass peaks corresponding to π^0 (401 events) and η (34 events). These events were contained within $3\cdot\sigma$ cuts. When an additional $3\cdot\sigma_{M_n}$ cut was made on the missing recoil neutron mass only two events resulted under η peak (Fig.19b), the suppression is $\zeta \approx 10^{-5}$. Using the branching ratios and CLAS acceptances, the resulting ratio of $ep \rightarrow e'\hat{X}^+$ to background count rates is $\approx 25\%$.

A similar estimation for the $\pi^+\eta'$ final state of (1) resulted in an upper limit for background contribution of $< 20\%$.

8.2. Coherent Background

Coherent background arises from production of conventional mesons that decay to the specific final states in (1) and (2). However only a limited number of them, i.e., those with natural spatial and C parity, (i.e., $J^{PC} = 0^{++}$, 1^{-+}, 2^{++})...., decay to $\pi\eta$ or $\pi\eta'$ final states. The decay angular distribution partial wave analysis that is necessary for the $J^{PC} = 1^{-+}$ exotics will permit additional identification of these conventional mesons (see end of Sec.3).

Among the well known mesons in the mass range $m_M \geq 1.3GeV$ only the 2^{++} $a_2(1320)$ has a large relative with and branching ratio to $\pi\eta$ (see Appendix B).

There are no known mesons with significant branching ratio to the $\pi\eta'$ final state. (Br$(a_2(1320) \rightarrow \pi\eta') < 1\%$ [34]).

Hence the $a2(1320)$ appears to be the only other meson in this mass range having the final states of reactions (1) and (2). In previous experiments with π beams (see Sec.2) the signature of exotics was found in accompaniment with the a_2[15,16,21]. In the Table 1. we show the estimated rate for $a_2^+(1320)$ electroproduction under the

same kinematic conditions and decay meson systems as the exotic production. The estimated statistics will allow reliable analysis to determine the hybrid and $a2(1320)$ meson properties.

9. Summary

The quark model allows the existence of hybrids, hadrons having a constituent gluon in addition to the constituent quarks. Hybrid mesons can have exotic J^{PC} or J^{PG} quantum numbers, unequal to those of a $q\bar{q}$ pair. Such mesons offer a unique signal of hybrids. A variety of hadronic, e^+e^-, Primakoff production, pion induced production in a nuclear coulombic field, and J/ψ decay experiments have ambiguous indications of hybrids. Two photoproduction experiments, detecting $b_1\pi$ and $\rho\pi$ decay channels, yielded similar results. Electroproduction experiments have not been reported.

This experiment will search for a $\hat{X}^{\dagger 0}$, $J^{PC} = 1^{-+}$, $J^{PG} = 1^{--}$exotic hybrid meson in electroproduction using the Hall B CLAS detector. The mass range of $\hat{X}^{+(0)}$ will be up to $\approx 2\ GeV$. The hybrid will be unambiguously reconstructed through the $\eta\pi^{+(0)}$ and $\eta'\pi^{+(0)}$ decay channels. In addition the zero spins of the decay channel mesons permit unique determination of the J and P of the exotic hybrid by measurement of the decay angular distribution, $W(\theta, \phi, \Phi)$. The polarization of the hybrid and hence the electroproduction helicity amplitudes can additionally be determined from $W(\theta, \phi, \Phi)$, giving a powerful tool in determining the production mechanism.

A thirty day run time period is requested at a beam energy of 6 GeV. Based upon a cross section upper limit obtained from charged $\hat{X}$ Primakoff production data and the assumption of predominance of pion t-channel exchange for $\hat{X}^+$ production, the number of reconstructed events is expected to be $\sim$ 5,000 - 10,000. (CLAS acceptance efficiencies for the final states are $\approx$ 5 $\rightarrow$ 10 %). The background count rate is expected to be in order of 1/4 of the signal. The electromagnetic production cross section of $\hat{X}^0$ cannot be estimated due to lack of data relating to diagrams having $\hat{X}^0$ vertices not violating C parity.

Because of the relatively large value of W used in the search, W $\leq$ 3 GeV, the CLAS magnetic field will set at half its nominal value in order to optimize acceptance of the outgoing e^-. Trigger requirements are an electron with one positive track. Target will be high pressure hydrogen gas.

10. Appendix A: Sensitivity to Photoproduction Amplitudes

Sensitivities to $\hat{X}$ production amplitudes obtained from $W(\theta, \phi, \Phi)$ measurements and characteristic of a 30 day run were estimated, (see Table 1). Photoproduction was chosen as illustrative. The $\hat{X}$ was assumed to lie above and interfere with the a_2. Equal widths were assumed for both mesons. The mass bin chosen for the decaying mesons was the lower quarter of the $\hat{X}$ mass distribution. It was positioned to overlap the upper quarter of the a_2 mass distribution. There were thus $\approx$ 5,000 analyzed events in the mass bin. The resulting phase angle between the $\hat{X}$ and the a_2 was $\approx 160°$ and was approximately constant. Assuming pion t - channel exchange results in the T matrix being diagonal in helicities. The decay angular distribution in the Gottfried Jackson frame is then:

$$W(\theta) \sim 5\, sin^2\theta\, \cos^2\theta + \mid a_T \mid^2 \sin^2\theta + 2\sqrt{5}\sin^2\theta\cos\theta\, \Re(a_T)$$

where a_T is the (complex) transverse amplitude of the $\hat{X}$ relative to the transverse a_2. $Re(a_T)$ is the real part of a_T. a_T was chosen = 0.3, resulting in a $\hat{X}$ cross section 1/10 that of the a_2.

A least squares fit was made to a simulation of the above decay angular distribution for the 5,000 events in the mass bin (4500 a_2, 500 $\hat{X}$). This is $\approx 1/5$ the estimated yield of $\hat{X}^+ \rightarrow \pi^+\eta$ given in Table 1. The width of the mass bin was chosen such that 1/4 of the Breit-Wigner distribution of each resonance was included. The resulting relative errors in the measured values of $\mid a_T \mid$ and $\frac{\Re(a_T)}{\mid a_T \mid}$ were 6 % and 3 % respectively.

The front-back asymmetry is, from the above expression for $W(\theta, \phi, \Phi)$:

$$\frac{3}{5}\,\frac{\sqrt{5}\; Re(a_T)}{2 + \mid a_T \mid^2}$$

For the amplitude values chosen above, the value of the asymmetry is $\approx$ 40 % with relative error $\approx$ 3 %.

Even though there may be substantial amplitude for $\hat{X}$ production, asymmetry measurements may be small in regions where a_T is mostly imaginary. Asymmetry measurements can, however, obtain $Im(a_T)$ from the photon transverse - transverse interference parts in polarized real photoproduction and electroproduction.

11. Appendix B:

Photo and Electroproduction Cross Sections

Assuming that the electromagnetic production of both the hybrid $\hat{X}$ ($J^{PC} = 1^{-+}$) and a_2 is by π t-channel exchange, upper limits to $J^{PC} = 1^{-+}$hybrid photoproduction

cross section can be estimated by using radiative decay widths and the a_2 photoproduction cross section[28]:

$$\sigma^{\gamma}_{\hat{X}} = \frac{3 \cdot \Gamma(\hat{X} \rightarrow \gamma\pi)}{5 \cdot \Gamma(a_2 \rightarrow \gamma\pi)} \cdot \sigma^{\gamma}_{a_2} \tag{1}$$

The assumption of π t-channel exchange in $a_2(1320)$ photoproduction is based upon measurements [35] indicating the predominance of this diagram. For $\hat{X}$ photoproduction, as mentioned earlier, Primakoff production is thought to be dominated by a similar t channel exchange with $\gamma \Leftrightarrow \pi$. The values of the γ and π propagators are approximately equal since $m_\pi^2 \approx m_\gamma^2 = 0$. Upper vertex form factor differences are negligible. The lower vertex, πNN, is obviously the same for both a_2 and $\hat{X}$ production. Eq.(10) is calculated for charged a_2^+ and ($\hat{\rho}^+ = \hat{X}^+$) hybrid states.

The radiative width of the a_2 is known[34]:

$$\Gamma(a_2 \rightarrow \gamma\pi) \approx\ 300\ keV \tag{2}$$

An upper limit of 20 keV is used for $\Gamma(\hat{X} \rightarrow \gamma\pi) \cdot Br(\hat{X} \rightarrow \eta\pi)$ (see Fig.4b). It is based[20] upon the measured $\hat{X} \rightarrow \rho\pi$ decay angular distribution in $\hat{X}$ Primakoff production in the $m_{\hat{X}}$ range of $\approx 1.1 \rightarrow 1.5$ GeV. Assuming reasonable 10% branching ratio for $\hat{X} \rightarrow \eta\pi$ we will have

$$\Gamma(\hat{X} \rightarrow \gamma\pi) \approx\ 200\ keV \tag{3}$$

Note that for counting rate the value of $Br(\hat{X} \rightarrow \eta\pi)$ is not important.

The photoproduction cross section $\sigma^{\gamma}_{a_2}$ is obtained from the measurements of reaction $\gamma p = n a_2^+ = n\rho^0\pi^+ = n\pi^+\pi^+\pi^-$ [35] in the energy range $E_\gamma = 3.7 \rightarrow 4.7\ GeV$ corresponding to the energy range of this proposal. It was measured:

$$\sigma^{\gamma}_{a_2^+ \rightarrow \rho^0\pi^+} \approx 0.8\mu b$$

After scaling by the known[34] branching ratios $Br(a_2^+ \rightarrow \rho^0\pi^+) = 0.35$ the $\gamma p \rightarrow a_2^+ n$ photoproduction total cross section was determined:

$$\sigma_{\gamma p \rightarrow a_2^+} = 2.3\mu b \tag{4}$$

Then using the values (2), (3) and (4) in equation (1):

$$\sigma_{\gamma p \rightarrow \hat{X}^+ n} \leq 0.9\mu b \tag{5}$$

The estimated $\hat{X}$ photoproduction cross section can be extended to electroproduction by expressing $\sigma_{ep \rightarrow \hat{X}^+ n}$ in terms of its longitudinal and transverse components σ_L and σ_T:

$$\frac{d^2\sigma_{\gamma p \rightarrow \hat{X}^+ n}}{dQ^2 dW} = \Gamma_e \cdot (\sigma_T + \epsilon\sigma_L) \tag{6}$$

where Γ_e is the Mott cross section, i.e., flux of transverse virtual photons

$$\Gamma_e = \frac{\alpha}{4\pi} \cdot \frac{W^2 - m^2}{m^2 E^2} \cdot \frac{W}{Q^2} \cdot \frac{1}{1-\epsilon} \tag{7}$$

ϵ is the virtual photon polarization parameter

$$\epsilon = \left(1 + 2\frac{Q^2 + \nu^2}{4EE' - Q^2}\right)^{-1} \tag{8}$$

and E, E' and m are initial and scattered electron energies and the proton mass, respectively and $\nu = E - E'$.

The VMD formalism can be used to approximate σ_T and σ_L. We use the Sakurai model[36]. It is a convenient hadronically based approximation in which the incident virtual photon is converted to a vector meson (VM) which has the same quantum numbers as the γ_V (vector meson dominance, VMD). The transverse and longitudinal cross sections are:

$$\sigma_T = \left(\frac{e}{f_{VM}}\right)^2 \left(\frac{m_\rho^2}{m_\rho^2 + Q^2}\right)^2 \cdot \sigma^T_{VM\ p\to X'+n} \tag{9}$$

$$\sigma_L = \left(\frac{e}{f_{VM}}\right)^2 \left(\frac{m_\rho^2}{m_\rho^2 + Q^2}\right)^2 \cdot \frac{Q^2}{m_\rho^2} \cdot (1-x)^2 \cdot \xi(Q^2,\nu) \cdot \sigma^T_{VM\ p\to X'+n} \tag{10}$$

The factor $\left(\frac{e}{f_\rho}\right)^2 \frac{m_\rho^2}{m_\rho^2+Q^2}$ describes the VMD process $\gamma \to \rho$; the denominator on the right is the (off shell) ρ propagator; the other terms describes the $\gamma\rho$ vertex[37]. $\frac{Q^2}{m_\rho^2}$ is the longitudinal component of a relativistic spin 1 state in the Lorentz gauge; see, e.g., Ref. [38], $x = \frac{Q^2}{2m\nu}$ the Bjorken scaling variable, m_ρ is the ρ mass. $\xi(Q^2,\nu)$ scales this model to the data. Vector meson electroproduction measurements in the Q^2 range of this proposal are best describes $\xi(Q^2,\nu) \approx 0.5$ [39].

Inserting the expressions for σ_T and σ_L into (15) and expressing the VM cross sections in terms of photoproduction , i.e.,

$$\sigma^T_{VM\ p\to X'+n} = \left(\frac{e}{f_{VM}}\right)^{-2} \sigma^{photo}_{\gamma p\to X'+n} \tag{11}$$

we obtain the electroproduction cross section :

$$\frac{d^2\sigma_{ep\to X'+n}}{dQ^2 dW} = \Gamma_e \cdot F_\rho \cdot \sigma_{\gamma p} \tag{12}$$

where

$$F_\rho = \left(\frac{e}{f_\rho}\right)^2 \left(\frac{m_\rho^2}{m_\rho^2 + Q^2}\right)^2 \cdot \left(1 + \epsilon\frac{Q^2}{2m_\rho^2}(1-x)^2\right) \tag{13}$$

1. D.Horn and J.Mandula, *Phys. Rev. D17*, 1978, p898
2. T. H. Burnett and Stephen R. Sharpe, Annual Reviews of Nuclear Science, Vol. 40, p. 327
3. L. G. Landsberg, Physics of Atomic Nuclei, Vol. 57, p. 42 (1994)
4. N. Isgur, R. Kokoski and J. Paton, *Phys. Rev. Lett. 54*, 1985, p.869.
5. F. deViron and J. Weyers *Nucl. Phys. B185*, 1981, p.391.
6. I.I. Balitsky, D.I. Dyakonov and A.V. Yung, *Z Phys. C33*, 1986, p.265.
7. Zhenping Li, Hadrons '91, S. Oneda and D. C. Peaslee, Eds., World Scientific, 1992, p. 726
8. *Proc. of the 2nd Int. Conf. on Hadron Spectroscopy*, 1987, Tsukuba, Japan.
   Glueballs, Hybrids and Exotic Hadrons: Workshop, 1988, Upton, NY.
   Hadron-89: Proc. of the 3rd Int. Conf. on Hadron Spectroscopy, 1989, Ajaccio, Corsica.
   Hadron-91: Proc. of the 4th Int. Conf. on Hadron Spectroscopy, 1991, College Park, Maryland.
9. L. Landsberg, *Preprint of IHEP 91-180, Parts I and II* 1991, Protvino.
   S.-U. Chung, *Nucl. Phys. A473*, 1988, p.511; *Z Phys. C46*, 1990, p.111.
10. M. Chanowitz and S. Sharpe, *Nucl. Phys. B222*, 1983, p.211.
11. T. Barnes, F.E. Close and F. deViron, *Nucl. Phys. B224* 1983, p.241.
12. F. Close and H. Lipkin *Phys. Lett. B196*, 1987, p.245.
13. S.Taun at al. *Phys. Lett. B213*. 1988, p.537
14. M.Tanimoto *Phys. Rev D27*, 1983, p.2648
15. D. Alde et al., *Phys. Lett. B205*, 1988, p.397.
16. H. Aoyagi et al., *Phys. Lett. B314*, 1993, p.246.
17. M. Zielinski et al., *Phys. Rev. D30*, 1984, p.1855.
18. S. Cihangir et al. *Phys. Lett. B117*, 1982, p.119.
19. T. Ferbel et al., *Proceedings of the XVI-th Recontre de Moriond on New Flavors and Hadron Spectroscopy*, Les Arcs - Savois, 1981, p.373.
20. M. Zielinski *Z Phys. C34*, 1987, p.255.
21. G.M. Beladidze et al., *Phys. Lett. B313*, 1993, p.276;
22. M. Atkinson et al., *Z Phys. C34*, 1987, p.157;
23. G. Condo et al., *Phys. Rev. D43*, 1991, p.2787;
24. J. D. Jackson, Rev. Mod. Phys. Vol 37, p 484 (1965)
25. O.Dumbrajs et al., *Nucl. Phys. B216*, 1983, p277
26. H.Funsten and G.Gilfoyle, *Workshop on CEBAF at Higher Energies*, 1994, p97.
27. K.Schilling and G.Wolf, *Nucl. Phys. B61*, 1973, p381.
28. I. Aznauryan, *Preprint YERPHY-1428(15)-94*
29. B. Niczyporuk, CLAS simulation program SDA, private communication.
30. GEANT, CERN Library
31. K.Beard EC code CLAS-NOTE-94-002.
32. CELEG Event Generator, CLAS-NOTE-89-0004
33. LEPTO version 6.1, *The Lund Monte Carlo for Deep Inelastic Lepton-Nucleon Scattering*, TSL/ISV-92-0065, 1992

34. Review of Particle Properties, Phys. Rev. D50 p. 1174 (1994)
35. Y. Eisenberg et al., *Phys. Rev. D5*, 1972, p15.
36. J. Sakurai, *Phys. Rev. Lett. 22*, 1969, p981.
37. T. H. Bauer et al, Rev. Mod. Phys., Vol 50, p. 261 (1978)
38. H. Pilkuhn, "The Interactions of Hadrons", North-Holland, 1967
39. D. Cassel et al, Phys. Rev. D24, p. 2787 (1981), Fig.19

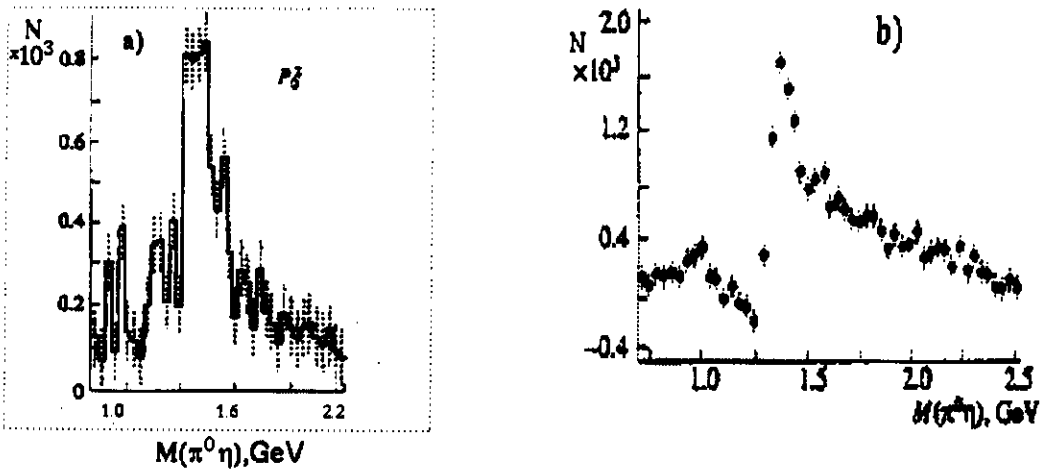

Figure 1: GAMS experiment: (a) - intensity distribution of the P_0 wave. (b) - dependance of forward-backward asymmetry in the GJ frame on invariant mass of $\eta\pi^0$ system.

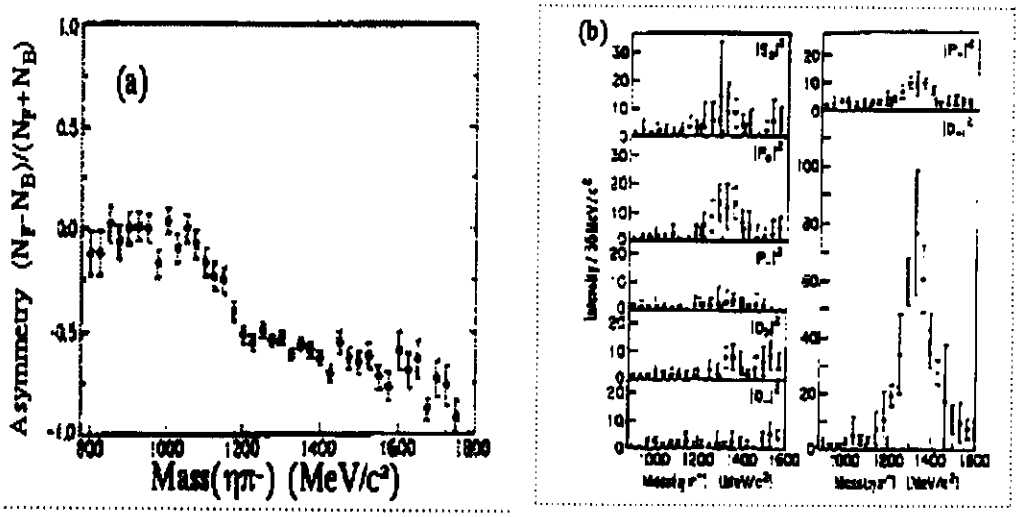

Figure 2: KEK experiment: (a)- Observed forward-backward asymmetry in the GJ frame. (b)- Intensity distributions of partial waves.

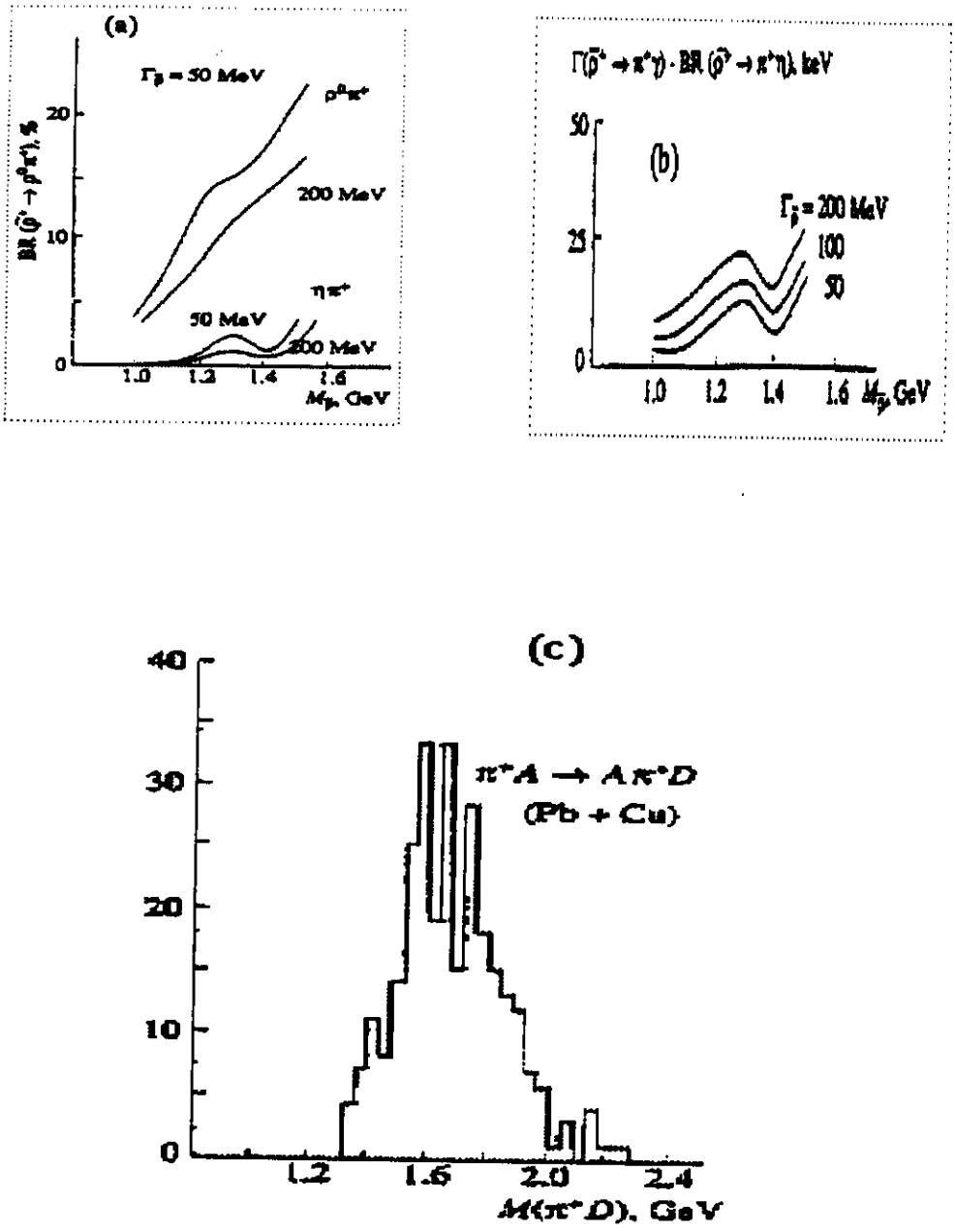

Figure 3: Estimated upper limits for the branching ratios and radiative widths for $\rho^0\pi^+$ - (a) and $\eta\pi^+$ - (b) final states in Primakoff production. (c) - observed peak in the π^+D system.

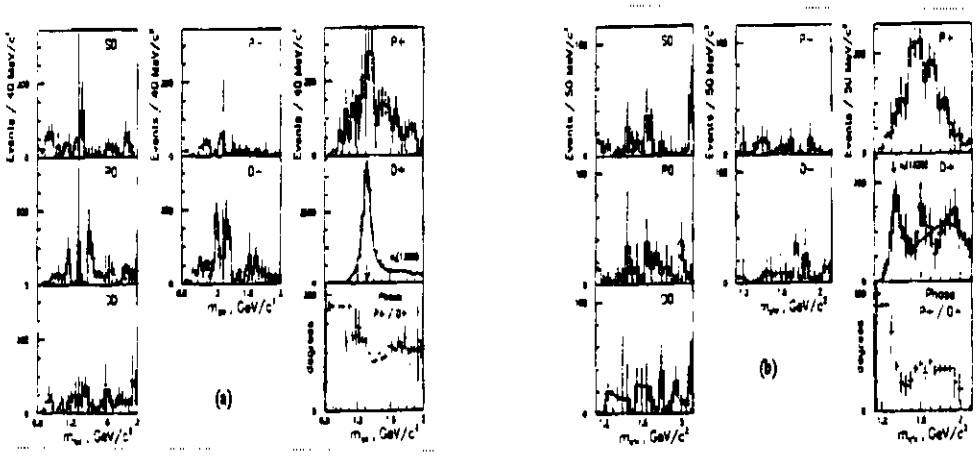

Figure 4: Results of the VES experiment. Partial wave intensity distribution in the (a) $\eta\pi$ and (b) $\eta'\pi$ decay meson systems.

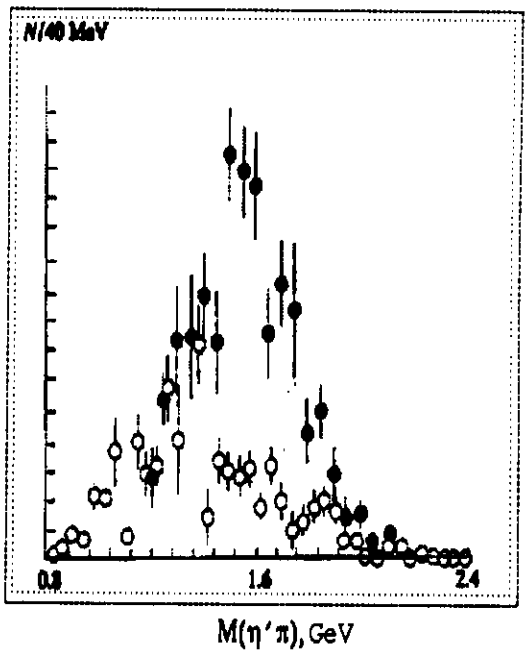

Figure 5: Matrix element squared of the P_+ wave in the $\eta\pi^-$ - o and $\eta'\pi^-$ - • systems.

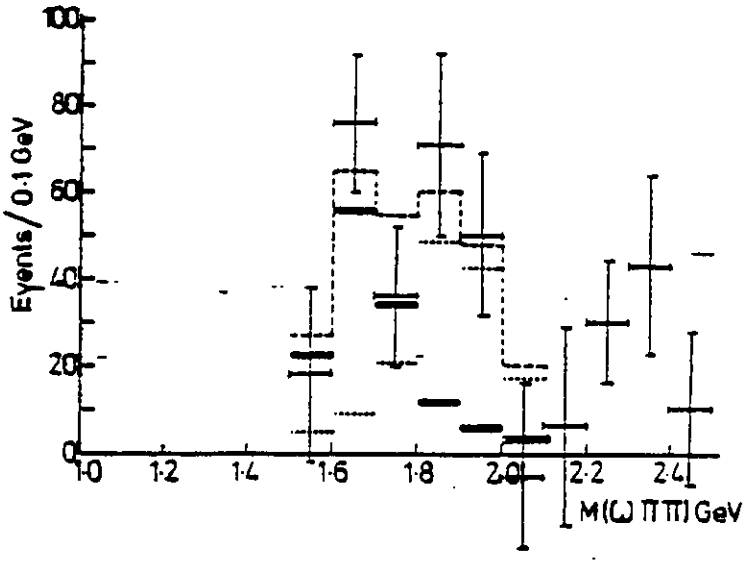

Figure 6: Yields of the reaction $\gamma p \Rightarrow \pi^+\pi^-\pi^+\pi^-\pi^0 p$ as a function of $\omega\pi\pi$ mass. o o o - contribution of ω_3, ... - contribution of another resonance.

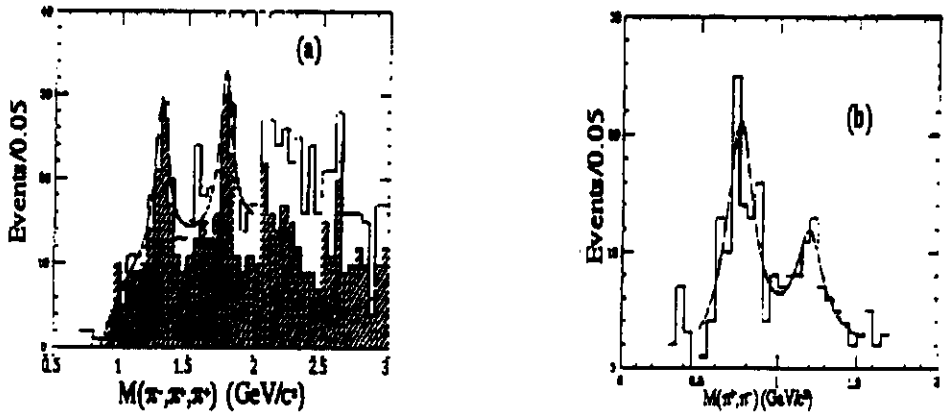

Figure 7: Distribution of events in the reaction $\gamma p \rightarrow \rho\pi^+ n \rightarrow n\pi^+\pi^+\pi^-$ as a function of M(3π (a). The $\pi^+\pi^-$ spectrum for events with $1.7 \leq M(3\pi) \leq 1.9 GeV$ (b).

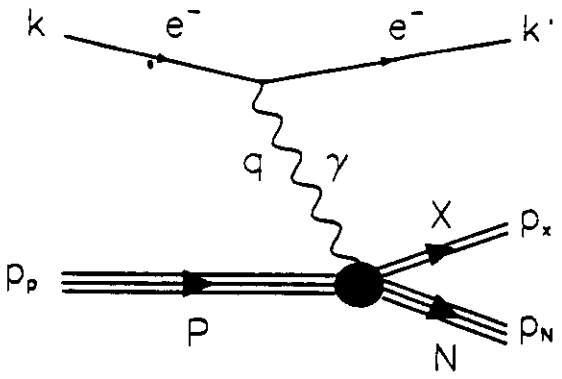

$q = (k - k')$

$W = (q + p_p)^2 = 2.6GeV - 3.1GeV$

$Q^2 = -q^2 > 0.7(GeV/c)^2$

Figure 8: One photon exchange diagram for meson electroproduction. k, k' and q are four-momenta of primary and scattered electrons and virtual photon, p_p, p_N and p_X are four-momenta of target proton, recoil nucleon and produced meson, respectively.

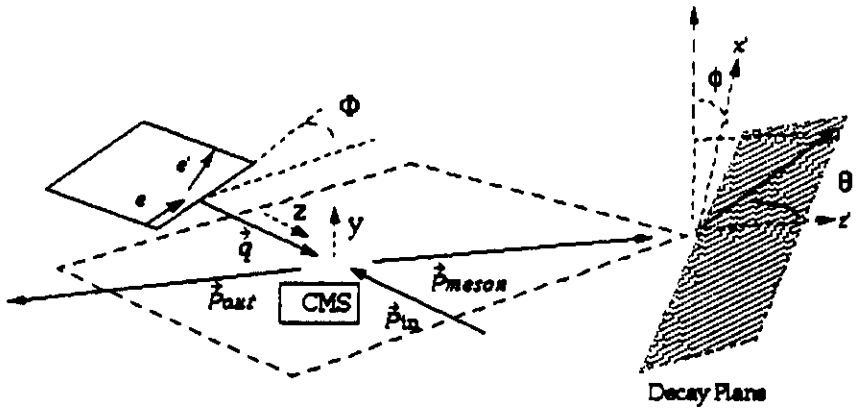

Figure 9: Electron scattering, hadron CMS (XYZ) and decay ($x'z'$) planes are shown. Φ is the angle between the electron and the hadron planes, θ is the polar angle of decay particle in the rest frame of decayed meson, ϕ is the angle between decay and $x'z'$ planes

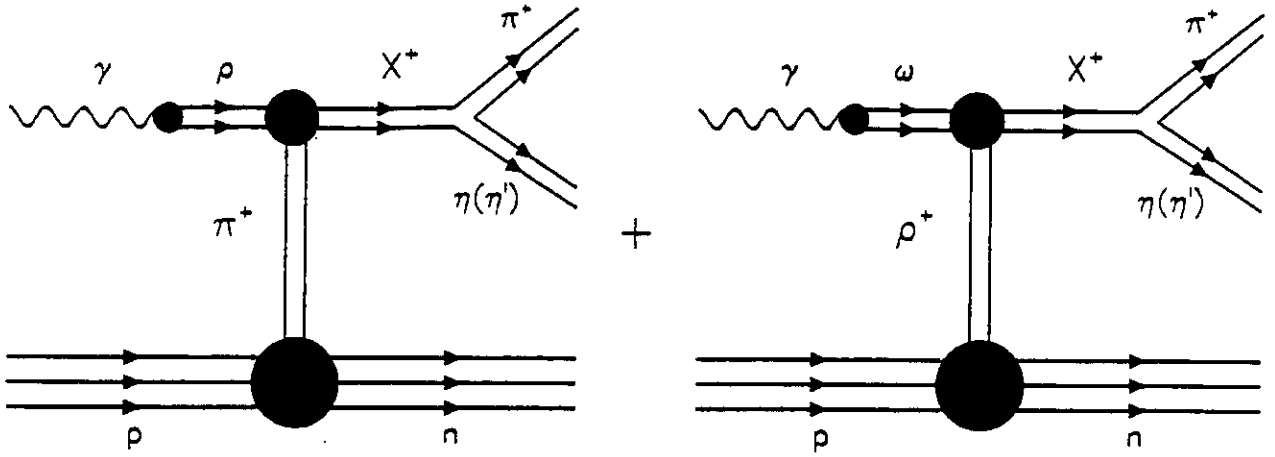

a)

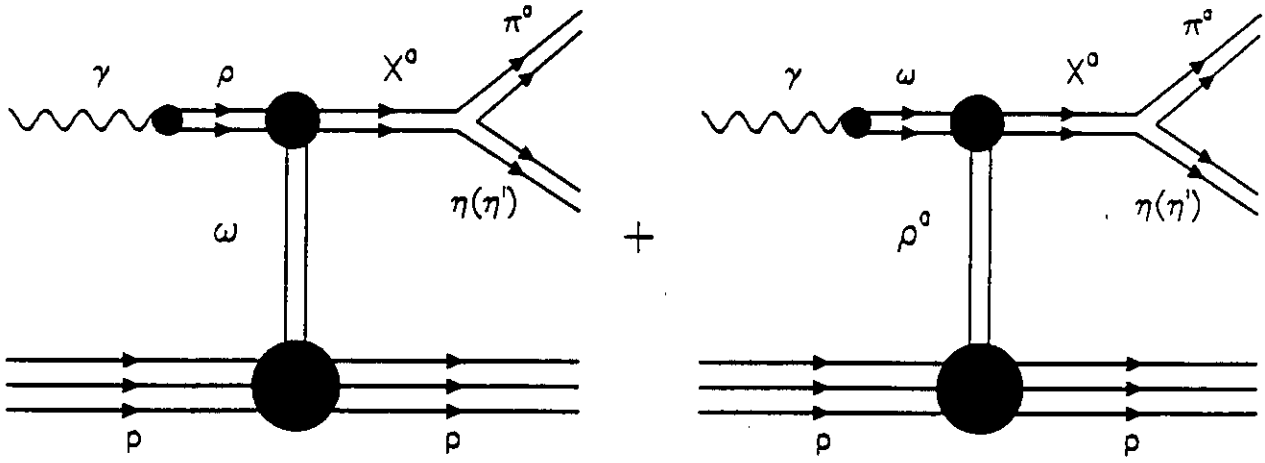

b)

Figure 10: Diagrams corresponding to the production of exotic mesons in the reactions $\gamma^* p \Rightarrow \hat{X} N$: (a) - $\hat{X}^+ \rightarrow \pi^+ \eta(\eta')$, (b) - $\hat{X}^0 \rightarrow \pi^0 \eta(\eta')$

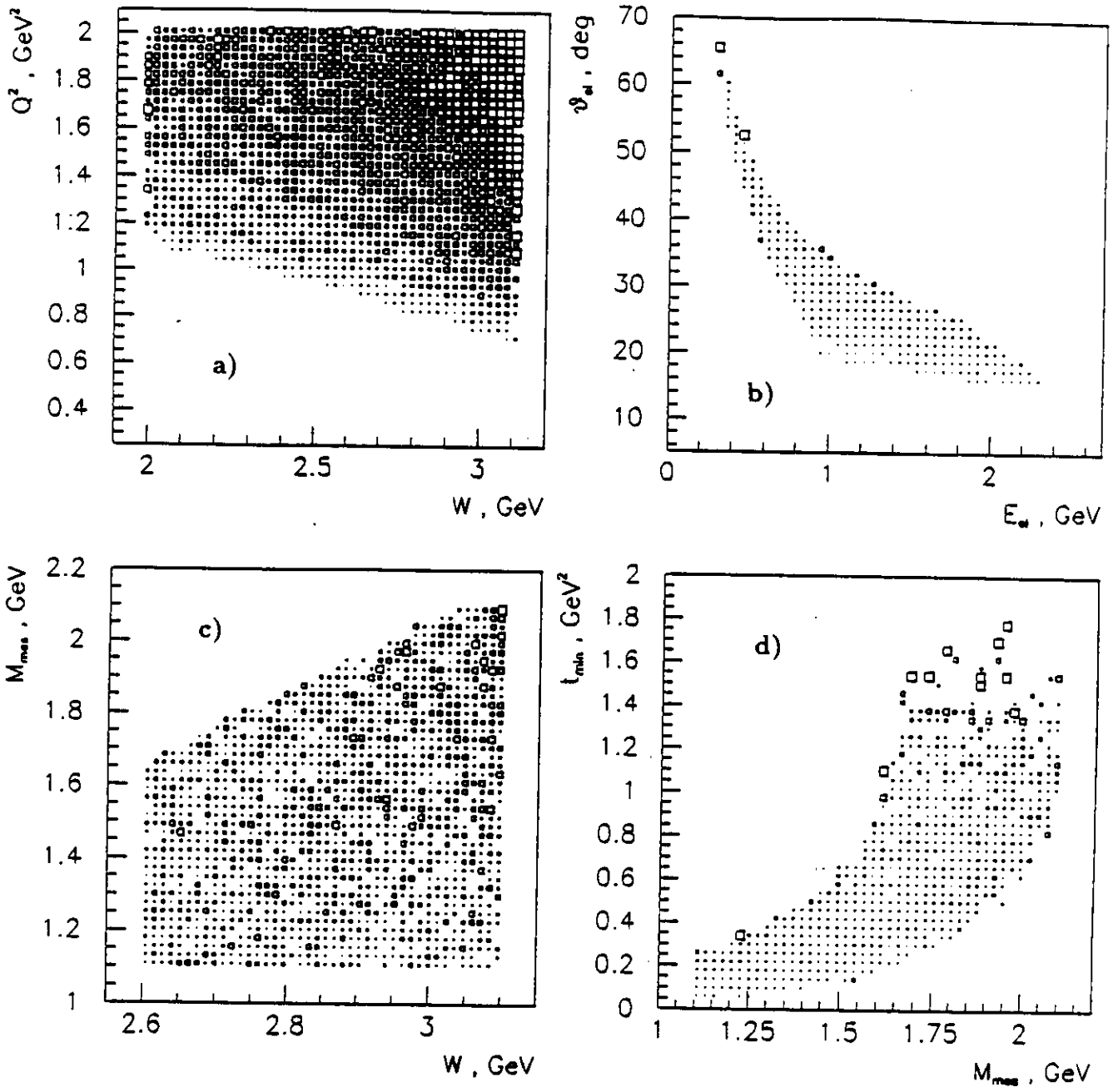

Figure 11: Simulation of kinematics for the reaction $ep \rightarrow e'\hat{X}N$ at a beam energy 6 GeV and 1/2 strength magnetic field. (a) - Q^2, W range accepted by CLAS, (b) - $M_{\hat{X}}$ acceptance for $W > 2.6$ GeV, (c) - scattered electron energy and polar angle distribution, (d) - minimum t v.s. measured hybrid mass for $W > 2.6$ GeV.

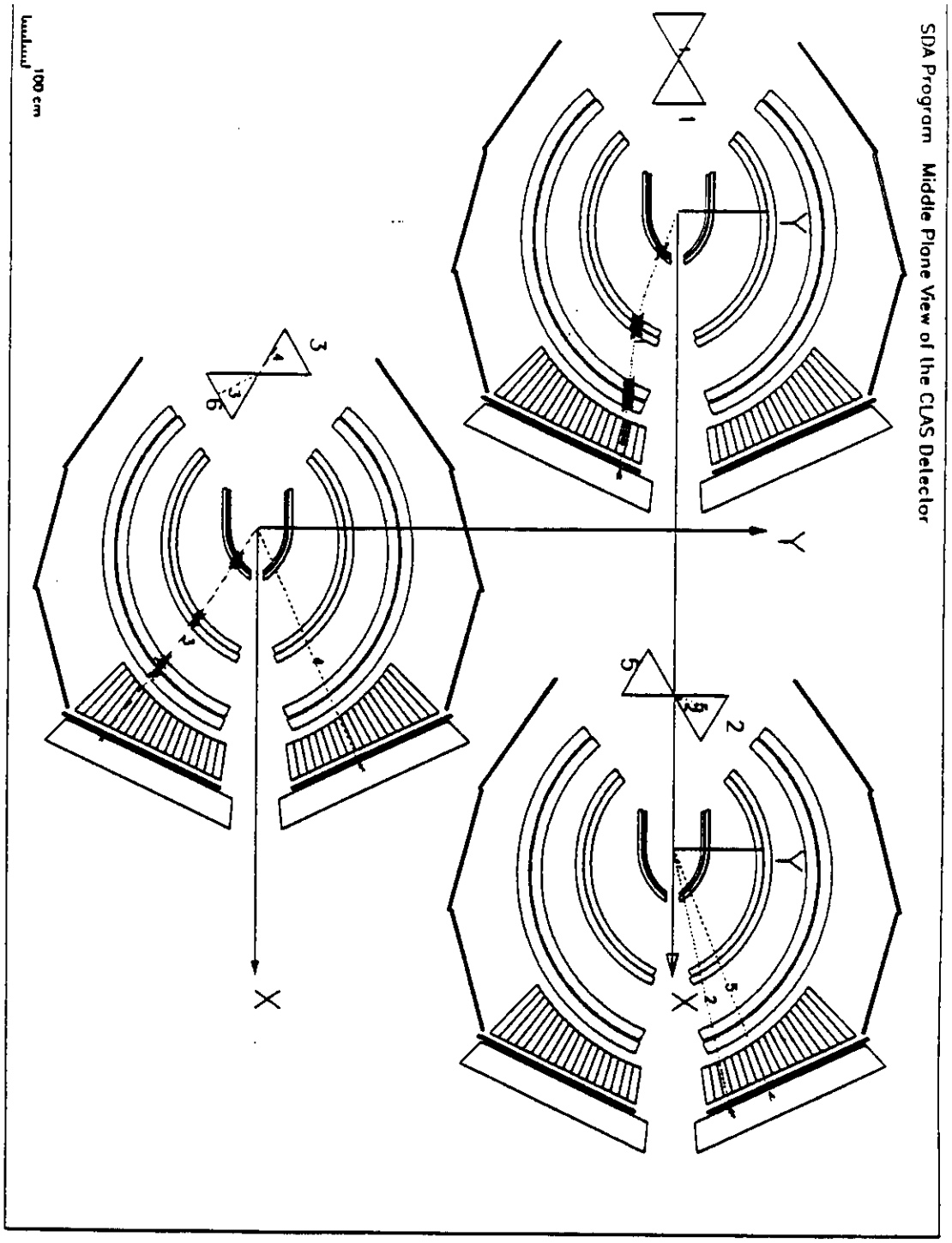

Figure 12: Simulated $ep \rightarrow e'\pi^+\gamma\gamma$ event in the CLAS detector: The tracks are labelled: 1 - electron, 2 - neutron, 3 - π^+, 4,5 - photons.

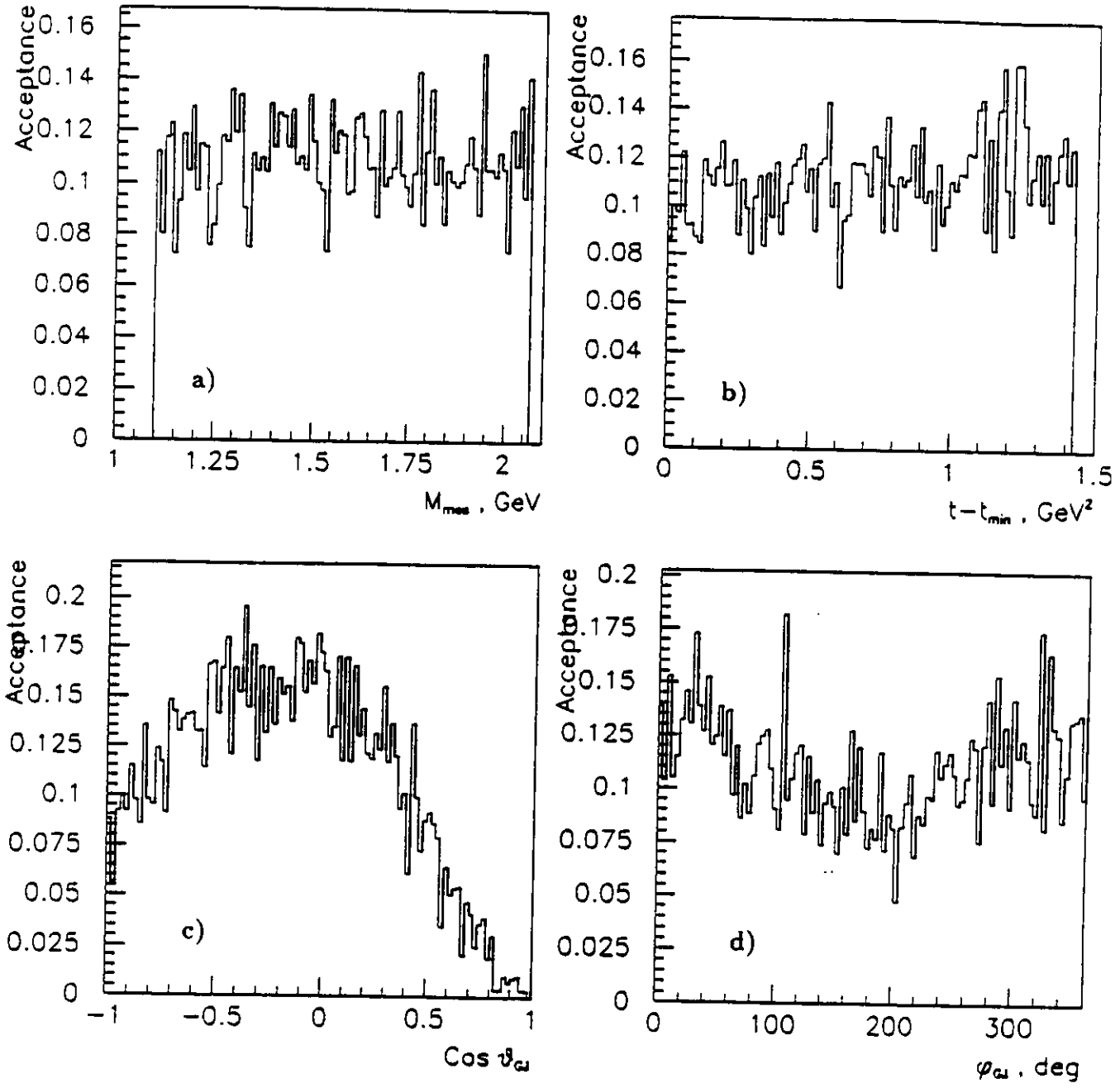

Figure 13: Dependance of CLAS acceptance for the $e'\pi^+\gamma\gamma$ final state: (a) - on invariant mass of $\pi^+\gamma\gamma$ system, (b) - on transfer momenta t, (c) and (d) - on polar and azimuthal angels in the GJ frame.

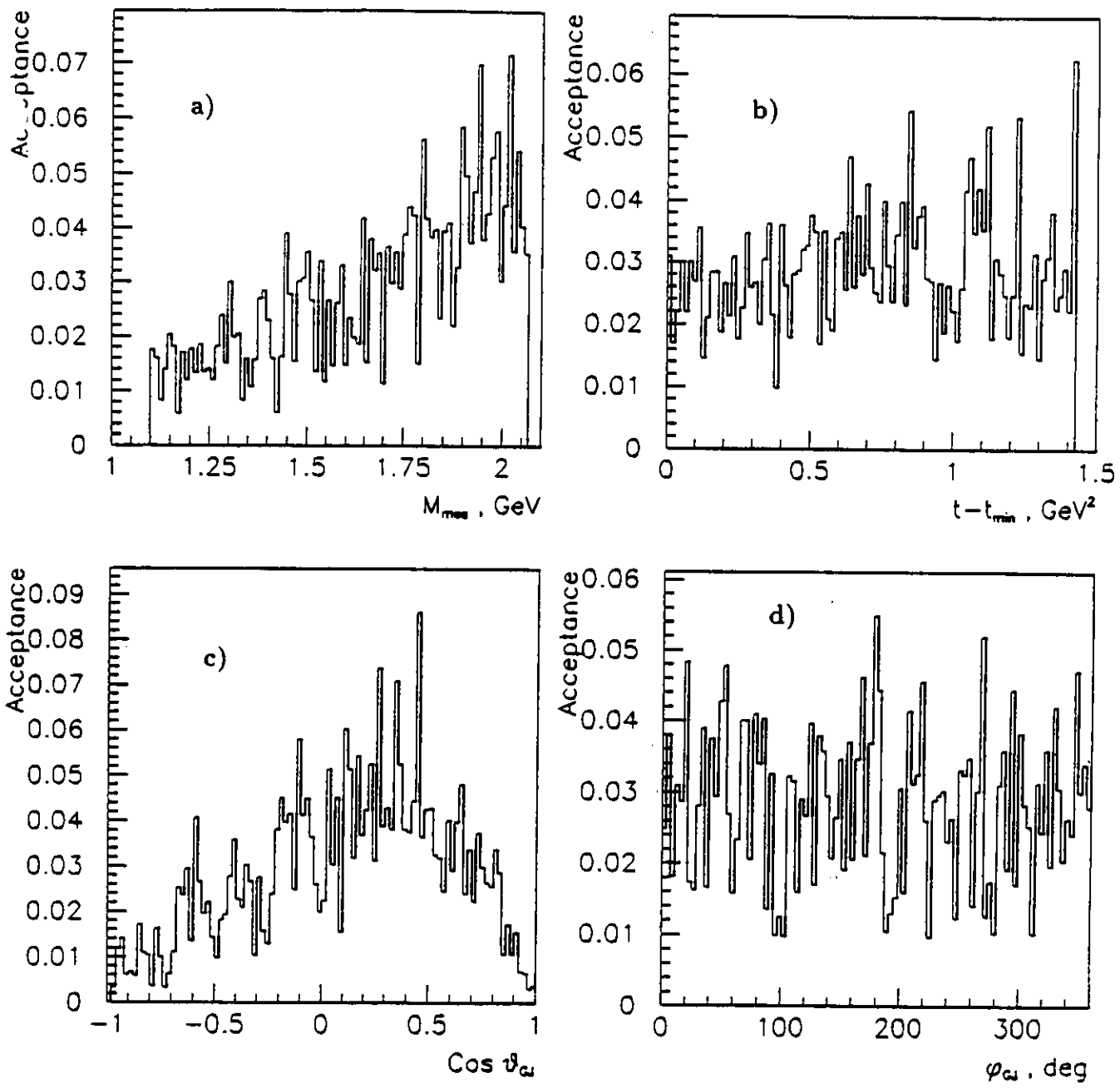

Figure 14: The same as in Fig.13 for the final state $e'\pi^+\pi^+\pi^-\gamma$.

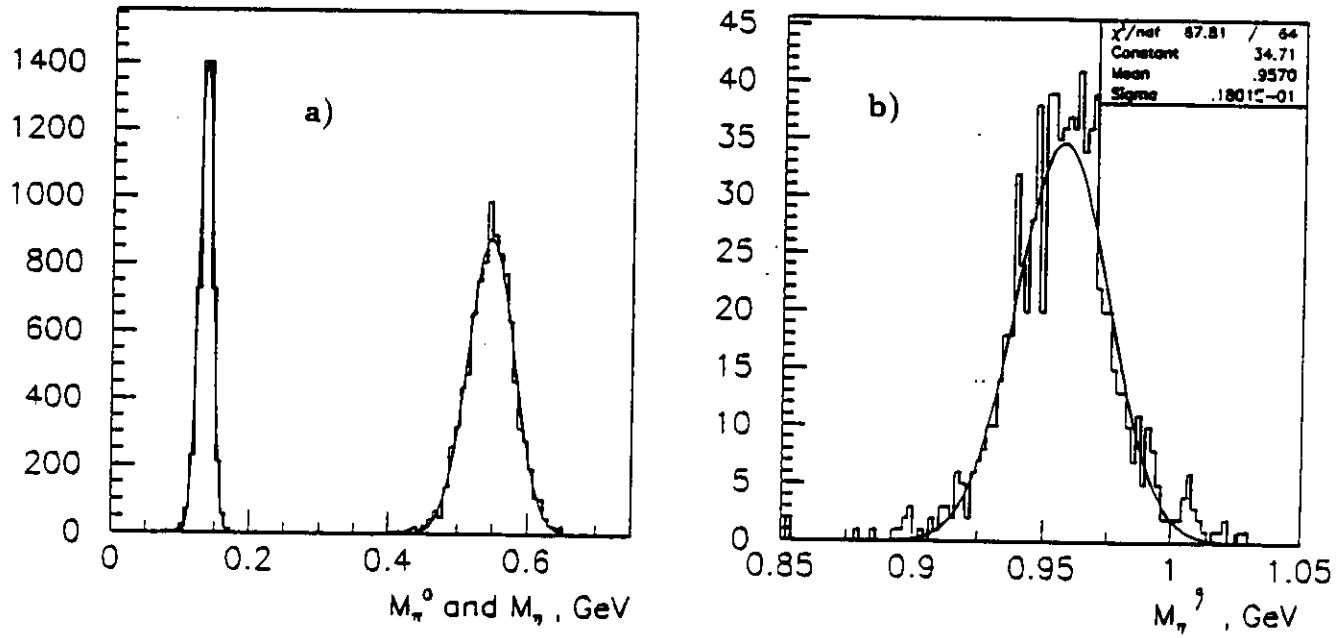

Figure 15: (a) - mass spectrum of reconstructed of π^0 ($\sigma_{\pi^0} = 17MeV$) and η ($\sigma_\eta = 35MeV$) from 2γ events, (b) - reconstructed η' ($\sigma_{\eta'} = 20MeV$) from $\pi^+\pi^-\gamma$ events.

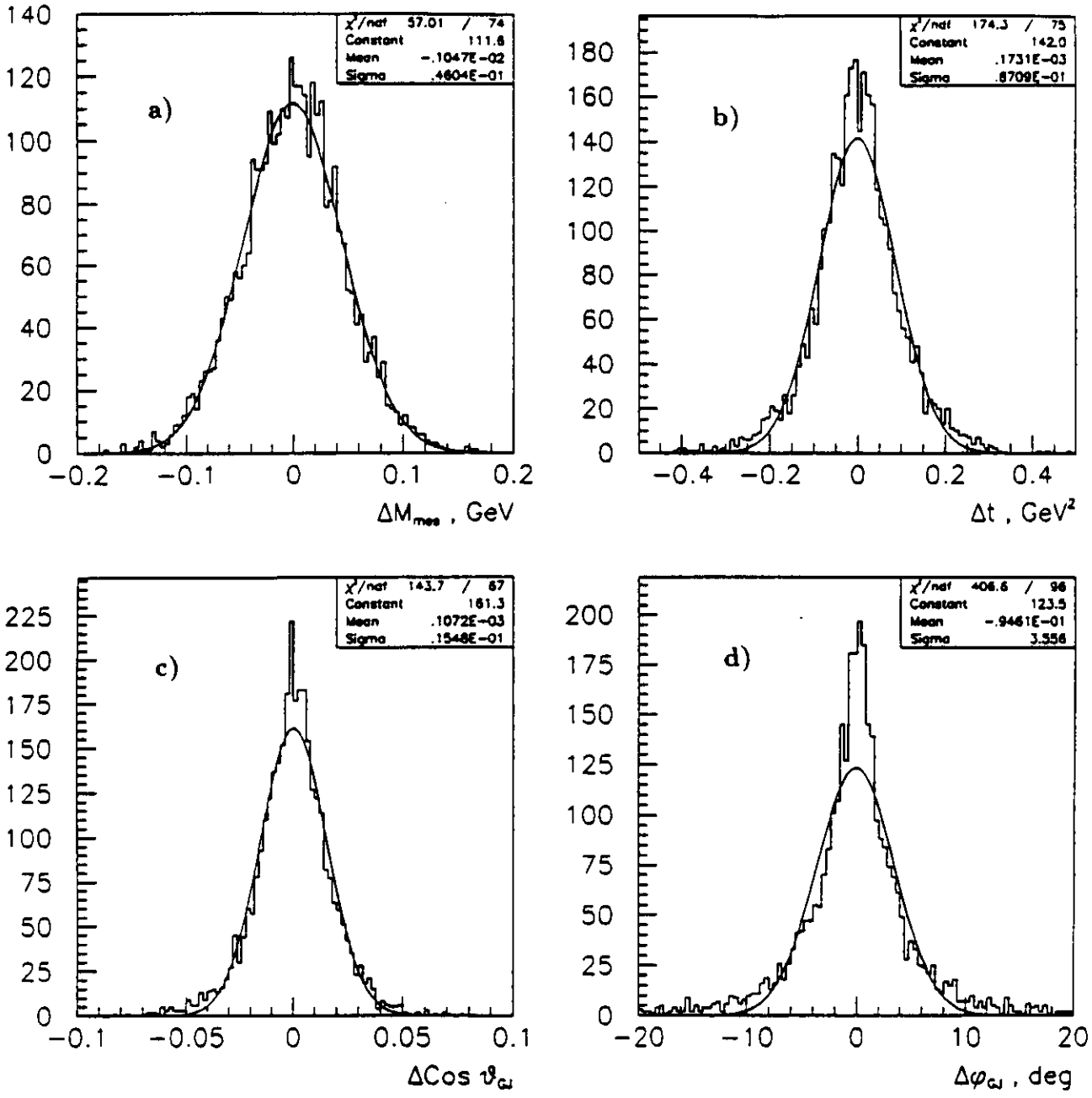

Figure 16: Simulated $M_{\hat{X}}$, t, θ_{GJ} and ϕ_{GJ} resolutions ((a), (b), (c) and (d) respectively) for the process $\hat{X} \to \pi^+\eta$.

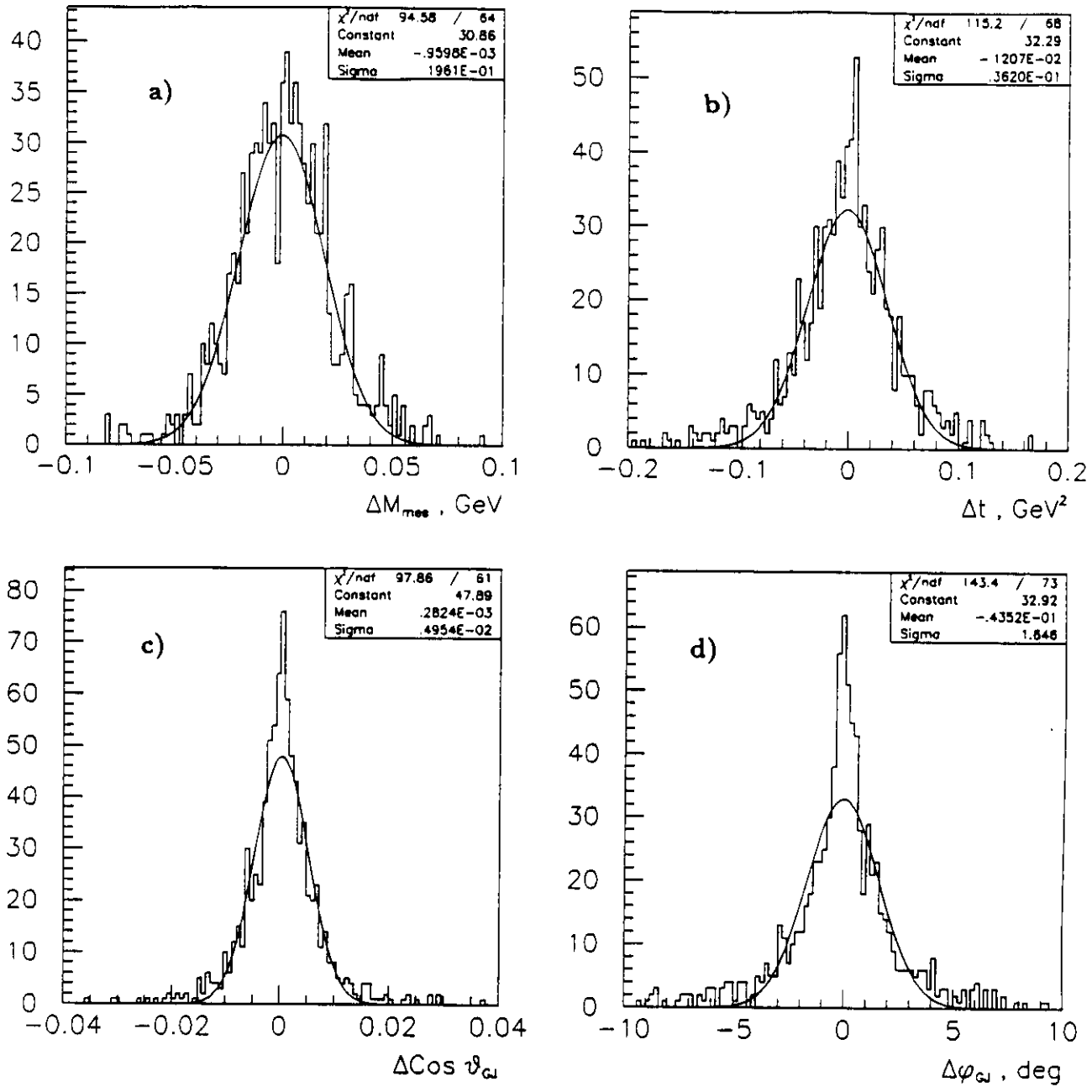

Figure 17: The same as in Fig.16 for the process $\hat{X} \to \pi^+\eta'$.

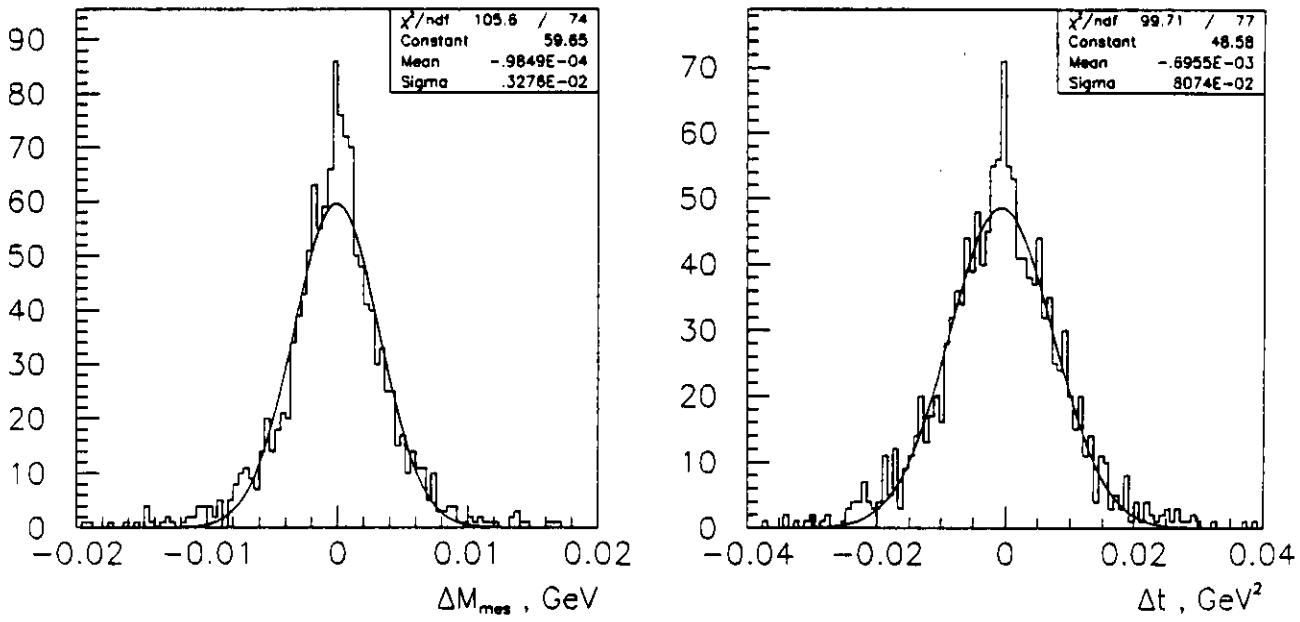

Figure 18: Resolutions of reconstructed $M_{\hat{X}}$ and t in the reaction $ep \rightarrow e'p\hat{X}^0$ from the detected proton.

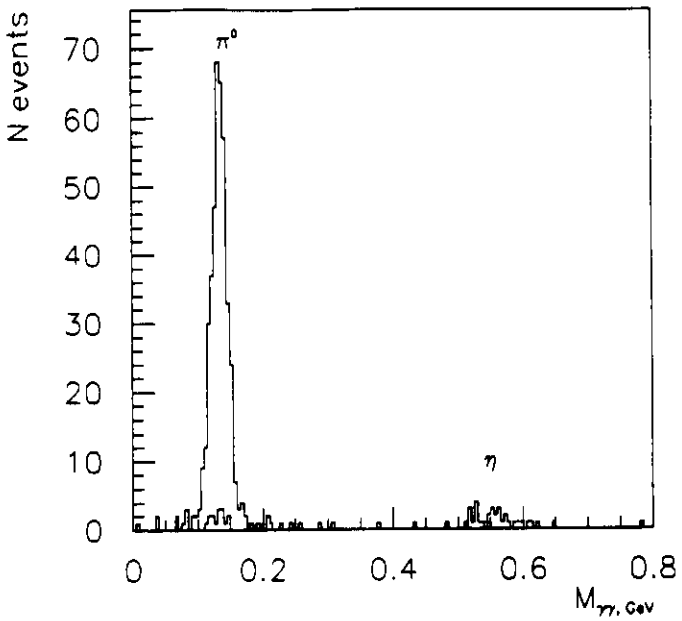

Figure 19: Reconstructed invariant mass spectrum of two photons detected by the electromagnetic shower calorimeter from simulated $e'\pi^+\gamma\gamma$ events.

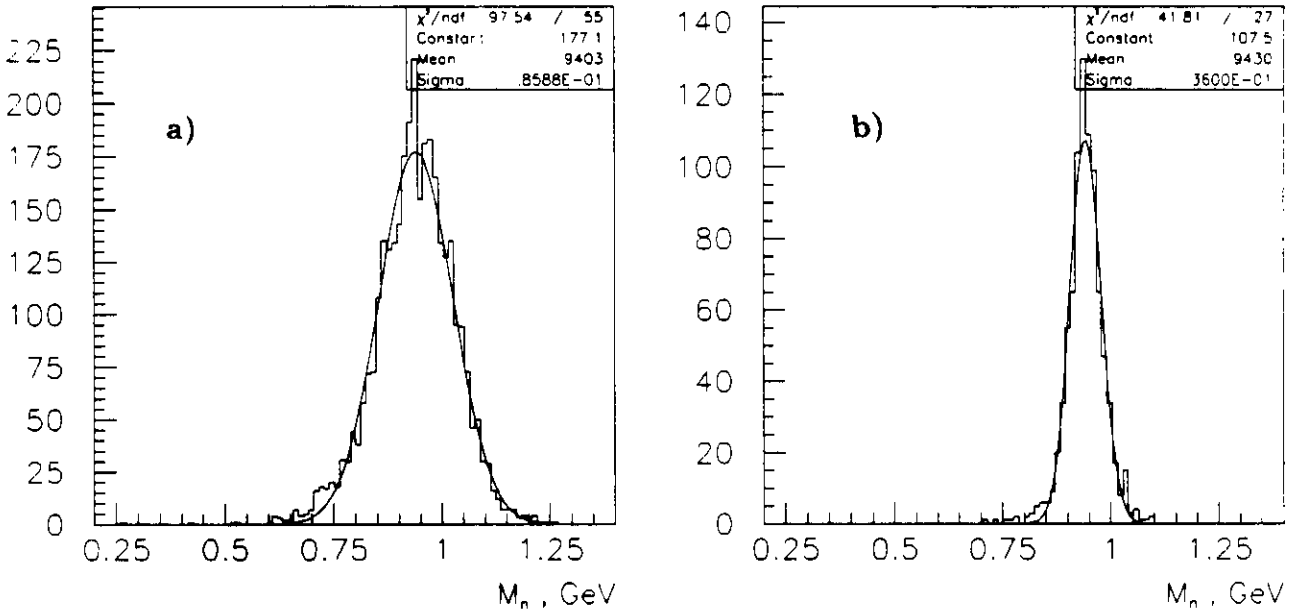

Figure 20: Reconstructed missing mass spectrum of neutrons in the reactions $ep \rightarrow e'\pi^+\gamma\gamma$ - (a) and $ep \rightarrow e'\pi^+\pi + \pi^-\gamma$ - (b).

HAZARD IDENTIFICATION CHECKLIST

CEBAF Proposal No.: _____ Date: _____
(For CEBAF User Liaison Office use only.)

Check all items for which there is an anticipated need.

Cryogenics
- _____ beamline magnets
- _____ analysis magnets
- _____ target
  - type: _____
  - flow rate: _____
  - capacity: _____

Electrical Equipment
- _____ cryo/electrical devices
- _____ capacitor banks
- _____ high voltage
- _____ exposed equipment

Radioactive/Hazardous Materials
List any radioactive or hazadorous/ toxic materials planned for use:
_____
_____
_____
_____

Pressure Vessels
- ~~5mm~~ inside diameter
- 20-50atm operating pressure
- kapton window material
- 10mg/cm^2 window thickness

Flammable Gas or Liquids
- type: Hydrogen
- flow rate: 0
- capacity: 100cc @ 1atm

Drift Chambers
- type: _____
- flow rate: _____
- capacity: _____

Other Target Materials
- ___ Beryllium (Be)
- ___ Lithium (Li)
- ___ Mercury (Hg)
- ___ Lead (Pb)
- ___ Tungsten (W)
- ___ Uranium (U)
- ___ Other (list below)

_____
_____

Vacuum Vessels
- _____ inside diameter
- _____ operating pressure
- _____ window material
- _____ window thickness

Radioactive Sources
- _____ permanent installation
- _____ temporary use
- type: _____
- strength: _____

Large Mech. Structure/System
- _____ lifting devices
- _____ motion controllers
- _____ scaffolding or
- _____ elevated platforms

Lasers
- type: _____
- wattage: _____
- class: _____

Installation:
- _____ permanent
- _____ temporary

Use:
- _____ calibration
- _____ alignment

Hazardous Materials
- ___ cyanide plating materials
- ___ scintillation oil (from)
- ___ PCBs
- ___ methane
- ___ TMAE
- ___ TEA
- ___ photographic developers
- ___ other (list below)

_____
_____

General:

Experiment Class:

- _____ Base Equipment
- _____ Temp. Mod. to Base Equip.
- _____ Permanent Mod. to Base Equipment
- _____ Major New Apparatus

Other: _____
_____

BEAM REQUIREMENTS LIST

CEBAF Proposal No.: _____ Date: _____
(For CEBAF User Liaison Office use only.)

List all combinations of anticipated targets and beam conditions required to execute the experiment. (This list will form the primary basis for the Radiation Safety Assesment Document (RSAD) calculations that must be performed for each experiment.)

Condition #	Beam Energy (MeV)	Beam Current (μA)	Polarization and Other Special Requirements (e.g., time structure)	Target Material (use multiple rows for complex targets — e.g., w/windows)	Target Material Thickness (mg/cm²)
1	6000	1 - 30nA	----	Hydrogen gas	200 - 500
1	6000	1 - 30	----	Kapton	10

The beam energies, E_{Beam}, available are: $E_{Beam} = N \times E_{Linac}$ where N = 1, 2, 3, 4, or 5. For 1995, E_{Linac} = 800 MeV, i.e., available E_{Beam} 800, 1600, 2400, 3200, and 4000 MeV. Starting in 1996, in an evolutionary way (and not necessarily in the order given) the following additional values of E_{Linac} will become available: E_{Linac} = 400, 500, 600, 700, 900, 1000, 1100, and 1200 MeV. The sequence and timing of the available resultant energies, E_{Beam}, will be determined by physics priorities and technical capabilities.

LAB RESOURCES REQUIREMENTS LIST

CEBAF Proposal No.: _____ Date: _____
(For CEBAF User Liaison Office use only)

List below significant resources — both equipment and human — that you are requesting *from CEBAF* in support of mounting and executing the proposed experiment. Do not include items that will be routinely supplied to all running experiments, such as the base equipment for the hall and technical support for routine operation, installation, and maintenance.

***Major Installations** (either your equip. or new equip. requested from CEBAF)*

_____

_____

_____

_____

_____

_____

_____

_____

_____

New Support Structures: _____

_____

_____

Data Acquisition/Reduction

Computing Resources: _____

_____

_____

New Software: _____

_____

_____

Major Equipment Standart CLAS equipment

Magnets _____

_____

Power Supplies _____

_____

Targets _____

_____

Detectors _____

_____

Electronics _____

_____

Computer Hardware _____

_____

Other _____

_____

Other

_____

_____

_____

_____

_____